3D drop deformation and breakup in simple shear flow considering the effect of insoluble surfactant.

S. Adami, X.Y. Hu and N.A. Adams
Institute of Aerodynamics
Technische Universität München
Garching, Germany
stefan.adami@tum.de

Abstract—We have developed a multi-phase SPH method to simulate arbitrary interfaces containing surface active agents (surfactants) that locally change the properties of the interface, such the surface tension coefficient [1]. Our method incorporates the effects of surface diffusion, transport of surfactant from/to the bulk phase to/from the interface and diffusion in the bulk phase. Neglecting transport mechanisms, we use this method to study the impact of insoluble surfactants on drop deformation and breakup in simple shear flow.

I. INTRODUCTION

Exposing drops to extensional flows such as e.g. a simple Couette flow, the viscous forces along the interface tend to deform the drop and elongate it to an ellipsoid-type shape. The balancing force to stop the deformation due to the shearing is the surface tension. When two pure fluids of different types are in contact, the resulting surface tension force is only proportional to the local curvature and normal to the interface. Depending on the strength of this force and the viscosity ratio between the two fluids λ, drops are deformed to a steady ellipsoid shape or break up. The correlation between the breakup behaviour and the flow parameter is known as the Grace curve [2].

Adding surface active agents (surfactants) to a multiphase system can strongly alter the flow phenomena. Neglecting the effect of such an additive on other material properties, surfactants mainly change the surface tension coefficients between two fluids when replacing fluid molecules at the interface with surfactant molecules. Hence, surface tension gradients along the interface can occur resulting in the so-called Marangoni forces [3].

Here, we only focus on the case of insoluble surfactants, i.e. surfactants are initially added to the interface and cannot dissolve to the adjacent fluid phases. Bazhlekov et al. [4] studied the effect of insoluble surfactants on drop deformation and breakup in simple shear flow with a boundary-integral method and clearly describe the different breakup modes. But due to the nature of their method, an interface capturing scheme is required and breakup is detected manually. By the use of a Lagrangian particle method we avoid these algorithms and handle interface deformations naturally.

In the following section we briefly introduce the governing equations for multiphase flows with surfactants. Exemplary we show a 3D simulation with steady deformation and validate it against analytical data. Finally we present a detailed study of the different breakup modes where we focus on the effect of tip streaming.

II. GOVERNING EQUATIONS

The isothermal Navier-Stokes equations are solved on a moving Lagrangian frame

$$\frac{d\rho}{dt} = -\rho \nabla \cdot \mathbf{v} , \qquad (1)$$

$$\frac{d\mathbf{v}}{dt} = \mathbf{g} + \frac{1}{\rho} \left[-\nabla p + \mathbf{F}^{(\nu)} + \mathbf{F}^{(s)} \right] , \qquad (2)$$

where ρ, p, $\mathbf{v}$, and $\mathbf{g}$ are material density, pressure, velocity and body force, respectively. $\mathbf{F}^{(\nu)}$ denotes the viscous force and $\mathbf{F}^{(s)}$ is the interfacial surface force.

Following the weakly-compressible approach [5], an equation of state (EOS) is used to relate the pressure to the density

$$p = p_0 \left(\frac{\rho}{\rho_0} \right)^{\gamma} + b , \qquad (3)$$

with $\gamma = 7$, the reference pressure p_0, the reference density ρ_0 and a parameter b. These parameters and the artificial speed of sound are chosen following a scale analysis presented by Morris et al. [6] which determines the threshold of the admissible density variation.

Assuming incompressibility, the viscous force $\mathbf{F}^{(\nu)}$ simplifies to

$$\mathbf{F}^{(\nu)} = \eta \nabla^2 \mathbf{v} , \qquad (4)$$

where η is the dynamic viscosity. Following the continuum-surface-tension model [7], the surface force can be expressed as the gradient of the surface stress tensor with the surface tension coefficient α

$$\mathbf{F}^{(s)} = \nabla \cdot [\alpha (\mathbf{I} - \mathbf{n} \otimes \mathbf{n}) \delta_\Sigma] = - (\alpha \kappa \mathbf{n} + \nabla_s \alpha) \delta_\Sigma . \qquad (5)$$

The Capillary force $\alpha \kappa \mathbf{n} \delta_\Sigma$ is calculated with the curvature κ, the normal vector of the interface $\mathbf{n}$ and the surface delta function δ_Σ. This expression describes the pressure jump condition normal to an interface. In case of surface tension variations along the interface (e.g., due to non-uniform temperature or surfactant concentration) the Marangoni force $\nabla_s \alpha \delta_\Sigma$ results

in a tangential stress acting along the interface (∇_s is the surface gradient operator $\nabla_s = (\mathbf{I} - \mathbf{n} \otimes \mathbf{n}) \nabla$).

Assuming insolubility in the phases, the evolution of surfactant on the interface is governed by a diffusion equation

$$\frac{d\Gamma}{dt} = \nabla_s \cdot \mathbf{D_s} \nabla_s \Gamma \ , \tag{6}$$

where Γ and $\mathbf{D_s}$ are the interfacial surfactant concentration and the diffusion coefficient matrix (in case of isotropic diffusion $\mathbf{D_s} = D_s \cdot \mathbf{I}$), respectively.

To close our model, we relate the interfacial surfactant concentration Γ to the surface-tension coefficient α by a constitutive equation. Widely used in literature, the Frumkin isotherm or the Langmuir model [8]–[12] are known to agree reasonably well with experimental data. But since we want to study the effect of surfactants very generally, here we use a simple linear relation between α and Γ.

III. NUMERICAL METHOD

We discretize our computational domain with Lagrangian SPH particles and solve the governing equations for these points using a quintic spline kernel. Here, we only briefly recall the main aspects and refer to Adami et al. [1] for the details of our method.

To ensure mass conservation in our multiphase SPH method we do not solve the continuity equation (1) but calculate the actual density of a particle via the sum

$$\rho_i = m_i \sum W_{ij} \ . \tag{7}$$

The indices i and j refer to the particle of interest i and its neighbours j, where the weighting function $W(x_i - x_j, h)$ is non-zero. The smoothing length h is set as constant and we usually choose $h = 1.5 * \Delta x$ (Δx is the initial particle spacing).

Following Hu and Adams [13], the acceleration of particle i due to the pressure and viscous force can be calculated from interactions with neighbouring particles according to

$$\frac{d\mathbf{v}_i^{(p)}}{dt} = -\frac{1}{m_i} \sum_j \left(V_i^2 + V_j^2 \right) \frac{\rho_j p_i + \rho_i p_j}{\rho_i + \rho_j} \nabla W (\mathbf{x}_i - \mathbf{x}_j) \tag{8}$$

and

$$\frac{d\mathbf{v}_i^{(\eta)}}{dt} = \frac{1}{m_i} \sum_j \left(V_i^2 + V_j^2 \right) \frac{2\eta_i \eta_j}{\eta_i + \eta_j} \frac{\mathbf{v}_i - \mathbf{v}_j}{|\mathbf{x}_i - \mathbf{x}_j|} \nabla W (\mathbf{x}_i - \mathbf{x}_j) \tag{9}$$

with m, V, η and $\nabla W(\mathbf{x}_i - \mathbf{x}_j)$ denoting the mass, volume, dynamic viscosity and the gradient of the kernel function, respectively.

To distinguish between particles of different fluid types we introduce a simple color function c that defines if a particle belongs to a phase ($c_i = 1$) or not ($c_i = 0$). Whenever particle i interacts with particles of another type, interface forces between them are calculated via

$$\frac{d\mathbf{v}_i^{(s)}}{dt} = -\frac{1}{m_i} \left(\alpha_i \kappa_i - \nabla_s \alpha_i \right) A_i \ , \tag{10}$$

where $\kappa_i = \nabla \cdot \mathbf{n}$ and $A_i = |\nabla c_i| V_i$ are the curvature and the interfacial length of a particle near an interface. The color gradient ∇c_i is obtained by an usual SPH gradient approximation and we find the normal direction at an interface from the normalized color gradients. For details of the surface tension force formulation we refer to [14].

Finally, we solve the surfactant diffusion equation on particles which have a non-zero color gradient, i.e. particles with neighbouring particles of another type. This ensures automatically the insolubility condition and surfactant remains on the interface during the entire simulation. Following [1] we find

$$\frac{dm_{si}}{dt} = \sum_j \left(\lambda_i V_i^2 + \lambda_j V_j^2 \right) \nabla W (\mathbf{x}_i - \mathbf{x}_j) \ , \tag{11}$$

where $\lambda = (\mathbf{I} - \mathbf{n} \otimes \mathbf{n}) D_s \nabla \Gamma |\nabla c|$ is the surfactant flux projected in tangential surface direction and D_s is the surface diffusivity of surfactant. For numerical reasons we further introduce a surfactant diffusion term in surface normal direction with the diffusion coefficient D_n, which helps to ensure smooth concentration profiles normal to the interface. This additional diffusion equation is required since a physical singularity at the interface is approximated numerically with a certain width and gradients in normal direction should be diffused.

Time integration is performed with a velocity-verlet scheme, where the time-step is chosen as the minimum of a CFL-condition, a viscous condition and a surface-tension condition, see [5], [15]. We use the Parallel Particle-Mesh (PPM) Library of Sbalzarini et al. [16] in our implementation which allows for large-scale simulations on parallel computer architectures.

IV. NUMERICAL EXAMPLES

In our first example we show a three-dimensional simulation of a drop that is exposed to a shear flow and deforms to a steady ellipsoid. At this sub-critical conditions the deformation can be calculated from a small-deformation theory by Taylor [17] and we show good agreement with our method. Introducing surfactants on the interface, we show that the deformation is strongly influenced and can completely change the behaviour of the droplet in the flow.

To visualize the results of our simulations we use the software *pv-meshless* [18]. We extended this powerful open-source package with some additional features to extract the deformation parameter of three-dimensional simulations.

A. Sub-critical drop deformation

We put a drop of size $R = 1$ in the middle of a periodic rectangular channel of size $L_x = 8R$, $L_y = 4R$ and $L_z = 4R$ and move the upper and lower wall boundaries with a velocity of $\pm u_\infty$. At the boundaries in x-,y- and z-direction we use periodic, symmetric and no-slip conditions, respectively. The drop and the bulk phase have both the same density $\rho_d = \rho_b = 1$. The capillary number Ca and the Reynolds number

Re are defined based on the shear rate $G = 2u_\infty/L_z$, i.e.

$$Ca = \frac{G\eta R}{\alpha}, \quad Re = \frac{\rho G R^2}{\eta}. \tag{12}$$

At small capillary and Reynolds numbers, the drop deforms to a steady ellipsoid. The deformation parameter $D = (a - b)/(a + b)$ with the transverse diameter a and the conjugate diameter b of the ellipsoid is used to quantify the steady deformation.
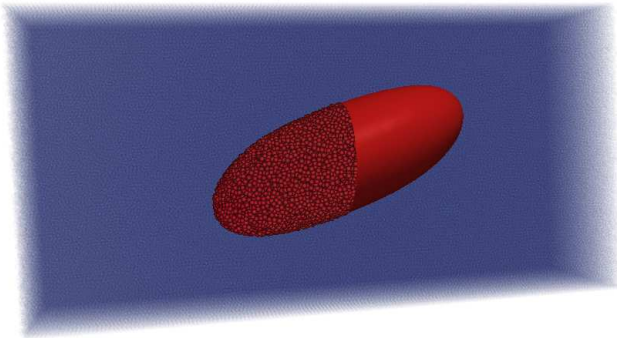
Fig. 1: Three-dimensional drop deformation in shear flow at $Re = 1$, $Ca = 0.2$ and a resolution of $3h = 0.15$ at $T = 25$.

In Fig. 1 we show the steady-state solution at $T = 25$ for a simulation with a resolution of $3h = 0.15$, i.e. a total of 1,024,000 particles. The capillary number is $Ca = 0.2$, hence the surface tension is strong compared to the shear forces and the drop deforms to a steady ellipsoid. The viscosity ratio $\Phi_\eta = \eta_d/\eta_b$ is set to one with a Reynolds number of $Re = 1$. The left half in Fig. 1 shows the actual particles and in the right half we show the extracted surface contour of the interface. Using this contour, we calculate the deformation D and plot it over time, see Fig. 2.
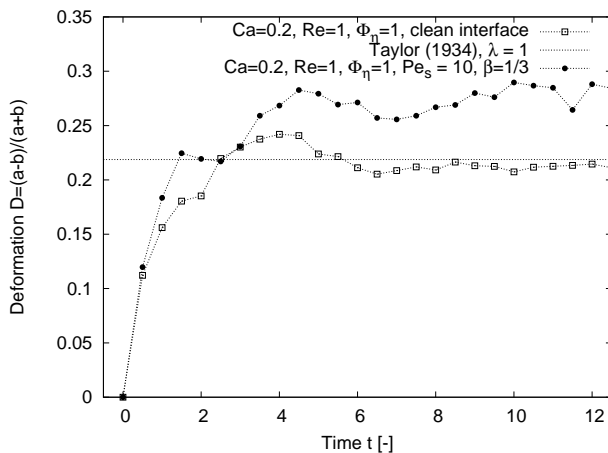
Fig. 2: Deformation parameter D over time for a drop in shear flow with and without surfactant at $Ca = 0.2$ and $Re = 1$.

The horizontal line in Fig. 2 shows the steady deformation predicted from the analytic expression of Taylor [17]

$$D = Ca \frac{16 + 19\Phi_\eta}{16 + 16\Phi_\eta} \tag{13}$$

with the parameter $Ca = 0.2$ and $\Phi_\eta = 1$. At early stages of the simulation, the initially spherical drop deforms transiently to an ellipsoid. Later, the steady deformation agrees well with the analytical prediction.

Now we study the effect of the presence of surfactants on a deforming interface for a drop in a shear flow at sub-critical conditions, i.e. where a steady deformation is reached. Therefore we simulate the same case with an initially uniform surfactant concentration on the interface of $\Gamma = 1$. The correlation between the surfactant concentration and the local surface tension coefficient is

$$\alpha\left(\Gamma\right) = \hat{\alpha}\left(1 - \beta\Gamma\right). \tag{14}$$

To avoid unphysical negative surface tension coefficients in Eq. 14 we use $\alpha\left(\Gamma\right) = max\left(\alpha\left(\Gamma\right), 0\right)$. In literature, other forms for this correlation are available with asymptotic behaviour at $\Gamma >> 1$, but for the purpose of general studies the simple piecewise defined function is appropriate.

The slope of the surface tension function β is taken to be $1/3$ and the maximum surface tension coefficient $\hat{\alpha}$ is 1.5-times the surface tension coefficient of the clean interface α_0. Hence, at an initial surfactant concentration of $\Gamma = 1$ the capillary number for the drop with surfactant is $Ca = 0.2$. The surface Peclet number Pe_s is defined as

$$Pe_s = \frac{GR^2}{D_s}, \tag{15}$$

which is the ratio of surfactant advection with the flow and diffusion along the interface with a diffusion coefficient D_s. Here, we use $Pe_s = 10$.

In Fig. 3 we compare the x-z plane through the center of the drop with and without surfactant at $T = 10$. The arrows denote the velocity field and are coloured with the magnitude of the velocity. For visibility we scaled all of them with a constant factor.

Due to the deformation of the drop, surfactant accumulates near the tips of the ellipsoid and the local concentration increases. Consequently, the surface tension is reduced and to balance the shear forces at the tips a higher curvature develops. That results in a higher deformation, see also the evolution of the deformation parameter with time for this case in Fig. 2. The more, the presence of the interfacial surfactant affects the internal flow and the inclination angle with the x-axis decreases.

At very low Peclet numbers, which is not shown here, an effect called "surface dilution" occurs. In that case diffusion is stronger than advection of surfactant to the tips, i.e. surfactant gradients are smoothed out very fast resulting in a nearly uniform surfactant concentration along the interface. As the total mass of surfactant does not change but the interfacial area increases, the uniform surfactant concentration is lower

(a) Clean interface
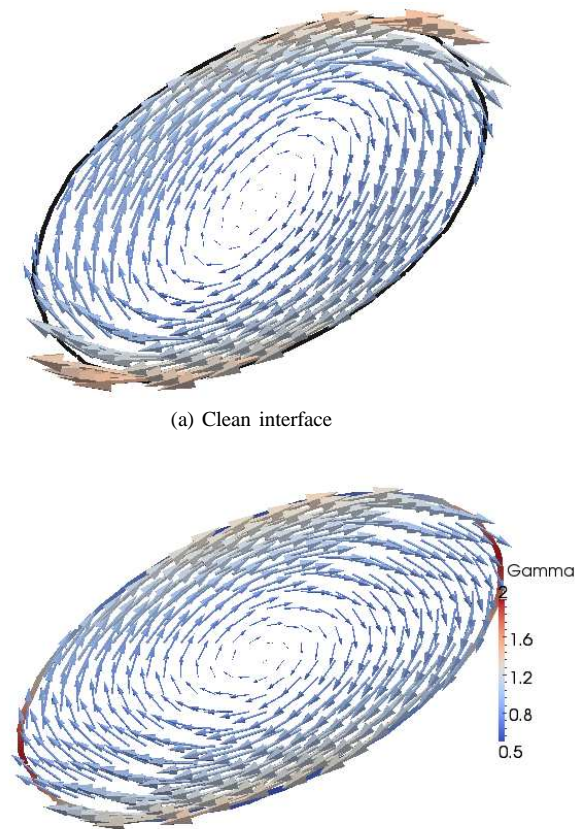
(b) Initial surfactant concentration $\Gamma = 1$, $Pe_s = 10$, $\beta = 1/3$ and $\hat{\alpha} = 1.5 \, \alpha_0$

Fig. 3: Velocity field and interfacial surfactant concentration in a x-z plane through the center of the drop with $Ca = 0.2$ and $Re = 1$ at $T = 10$.

than the initial concentration. Consequently, surface tension increases and the deformation is lower compared to the clean drop.

B. Super-critical drop deformation

When the shear forces are high compared to the surface tension force, the drop does not deform to a steady ellipsoid but breaks up into several smaller droplets. As a reference, we simulated a clean droplet in a large box with $L_x = 18R$, $L_y = 4R$ and $L_z = 4R$ at $Ca = 0.4$.
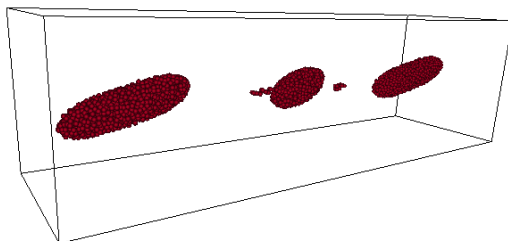
Fig. 4: Drop breakup in shear flow at $T = 50$ for a clean drop with $Ca = 0.4$ and $Re = 1$.

Fig. 4 shows a snapshot of the drop particles at $T = 50$ for the reference case. After initially forming a long neck, the drop breaks into several smaller droplets. These droplets are then steadily deformed since the length-scale of these droplets, hence the capillary number, is smaller.

Now we expose a surfactant enriched droplet with $\Gamma = 1$ and $Pe_s = 1$ to the same shear flow. In Fig. 5 three snapshots at $T = 10$, 30 and 50 show the extracted surface contour with a color map of the local surfactant concentration.

(a) T=10

(b) T=30

(c) T=50
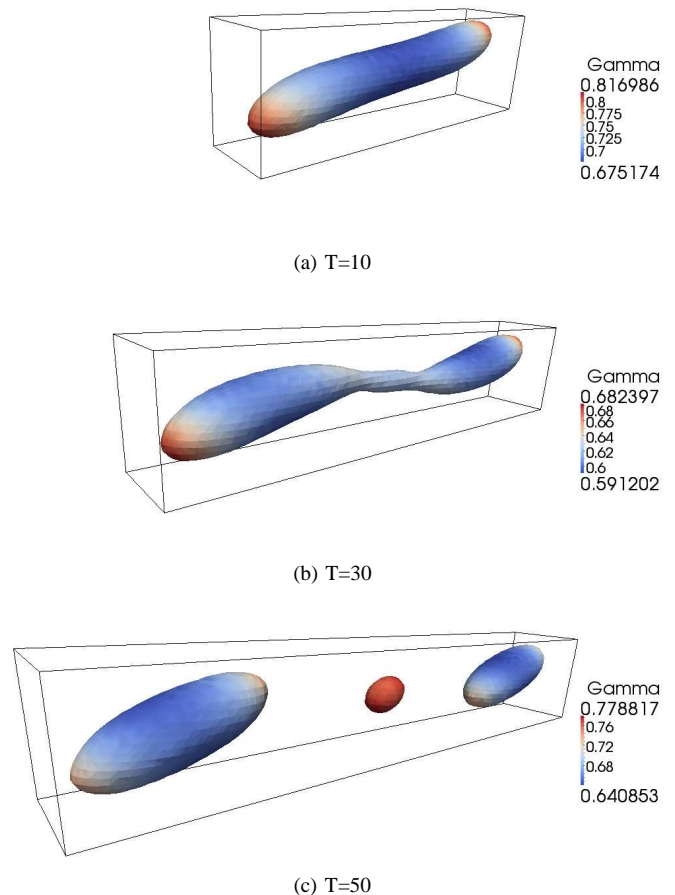
Fig. 5: Drop deformation and breakup in simple shear flow at $Ca = 0.4$, $Re = 1$ and $\Gamma = 1$: Extracted surface contour with a color-map of the local surfactant concentration at three different time steps.

Initially, the droplet strongly deforms and a neck is produced. As the interface is stretched but the total mass of surfactant does not change, the maximum surfactant concentration is lower than the initial concentration, see Fig. 5a. At later times, the neck becomes unstable and finally breaks up, see Fig. 5b and 5c. Note also that now the highest surfactant concentration occurs at the smallest droplet.

To further discuss the effect of surfactant during breakup we compare two snapshots of the droplet at $T = 35$ with a clean interface and a surfactant enriched interface. Fig. 6 shows the velocity field and the surfactant concentration in the x-z

(a) Clean interface

(b) [Initial surfactant concentration $\Gamma = 1$, $Pe_s = 1$, $\beta = 1/3$ and $\hat{\alpha} = 1.5\,\alpha_0$
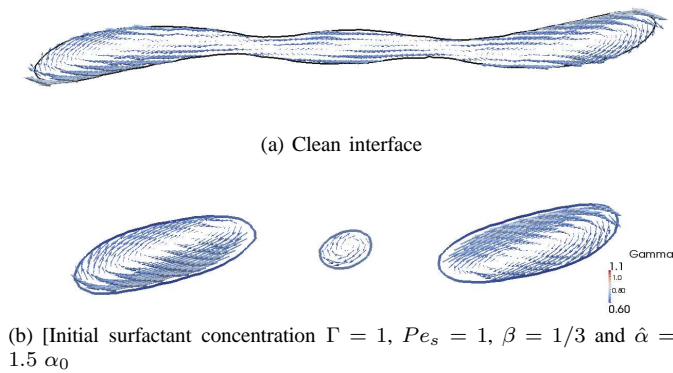
Fig. 6: Velocity field and interfacial surfactant concentration in a x-z plane through the center of the drop with $Ca = 0.4$ and $Re = 1$ at $T = 35$.

plane through the center of the drop for the two simulations. The drop with a clean interface is much further stretched and the unstable neck starts to narrow down. In contrast, the surfactant enriched drop already split up and three separate drops are formed. This example shows clearly the effect of the Marangoni force, which is the tangential force due to surface tension gradients on the interface. Initially surfactant is advected to the tips resulting in surfactant gradients. The resulting Marangoni forces try to retard the deformation, hence the extensional stretch is smaller compared to the clean interface. But as the neck becomes unstable like seen in Fig. 6a, the Marangoni effect amplifies the increasing curvature at the neck and the drop breaks up earlier. Not shown here, but note that on the other hand the fragments of the drop with surfactant are less deformed due to the surface dilution effect.

C. Tip streaming

When the Peclet number Pe_s is very high, diffusion of surfactant along the interface is negligible and mostly all of the surfactant is advected to the tips of the drop. Accordingly, surface tension at the tips drops to zero and there is no force to balance the viscous stress. This results in an unstable drop that breaks into very small droplet filaments at the tips.
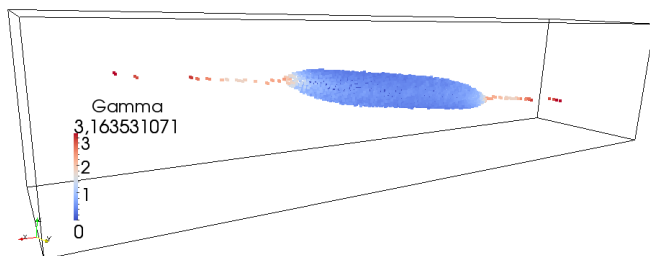
Fig. 7: tip streaming at $T = 11$

Fig. 7 shows a snapshot of the drop particles at $T = 11$. The surface Peclet number in this example is $Pe_s = 100$,

thus surface diffusion is very small. Accordingly, most of the surfactant is advected to the tips of the drop leading to locally very high concentrations. The maximum concentration is $\Gamma \approx 3$, see the legend in the figure. From the surface tension correlation $\alpha(\Gamma) = \hat{\alpha}(1 - \beta\Gamma)$ with $\beta = 1/3$ it follows that the surface tension at the tips is zero. As the viscous stress at the tips is not balanced by the surface tension force, the drop breaks at the tips and a filament of small droplets separates. This phenomenon is called *tip streaming*. As the tip stream carries a large portion of the surfactant mass away, the concentration on the main drop is strongly decreased thus surface tension is more dominant now. As a consequence, the remaining slightly smaller drop is steadily deformed at a smaller Capillary number compared to the initial status.

To explore the dominating effects during *tip streaming* and the *breakup* phenomenon, we performed several simulations at various Peclet numbers and different surface tension correlations. Fig. 8 shows the parameter range we studied and the corresponding breakup behaviour. Starting from the reference case with $Pe_s = 100$, $\Gamma = 1$, $\beta = 1/3$, $Ca = 0.4$ and $Re = 1$ we increase the surface diffusion and monitor the breakup behaviour. The smaller the Peclet number, the stronger is the surface diffusion to smooth out surfactant concentrations along the interface. At $Pe_s = 20$ a mixture of the tip streaming and drop breakup occurs and further decreasing Pe_s shows a pure breakup of the drop. Similar, with an increasing slope of the surface tension correlation β at the fixed Peclet number $Pe_s = 100$ we can manipulate the tip streaming and get a pure drop breakup. Note, the other parameter are adjusted to start with the same initial reference conditions. A high slope β means that small surfactant concentration gradients result in strong Marangoni forces. At $\beta > 0.125$ this effect is strong enough to retard the drop deformation and tip streaming does not occur even though surface diffusion is very small.
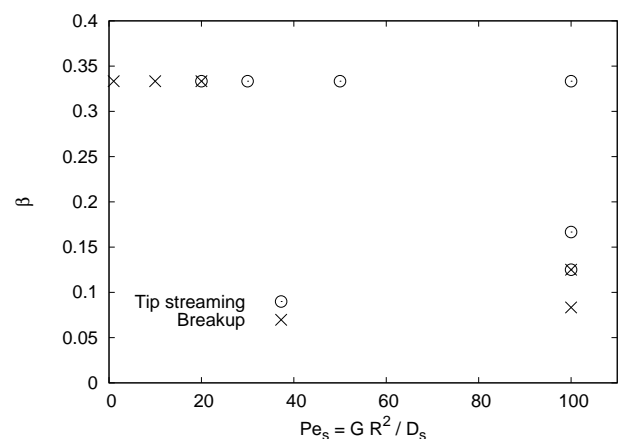
Fig. 8: Breakup behaviour at various Peclet numbers and different surface tension correlations.

V. Conclusion

We have developed a multiphase SPH method to simulate interfacial flows with surfactant dynamics. In the present study we only consider surface diffusion of insoluble surfactants, but even more complex transport phenomena as adsorption and coupling with bulk diffusion can be included. Our method conserves mass of surfactant exactly, which is of special importance for realistic long-term simulations. Comparison with analytic solutions shows validity of our method and the fully MPI-parallel implementation enables us to run complex large-scale simulations. Using this method, we have studied the three-dimensional drop deformation and breakup in simple shear flow with and without surfactants.

Acknowledgment

References

[1] S. Adami, X. Hu, and N. Adams, "A conservative SPH method for surfactant dynamics," *J. Comput. Phys.*, vol. 229, no. 5, pp. 1909 – 1926, 2010.

[2] H. Grace, "Dispersion phenomena in high viscosity immiscible fluid systems and application of static mixers as dispersion devices in such systems," *Chem. Engrg. Comm.*, vol. 14, no. 3, pp. 225–277, 1982.

[3] L. Scriven and C. Sternling, "The marangoni effects," *Nature*, vol. 187, no. 4733, pp. 186–188, 1960.

[4] I. Bazhlekov, P. Anderson, and H. Meijer, "Numerical investigation of the effect of insoluble surfactants on drop deformation and breakup in simple shear flow," *J. Colloid Interface Sci.*, vol. 298, no. 1, pp. 369–394, 2006.

[5] J. J. Monaghan, "Smoothed particle hydrodynamics," *Reports in Progress in Physics*, vol. 68, no. 8, pp. 1703–1759, 2005.

[6] J. Morris, P. Fox, and Y. Zhu, "Modeling low reynolds number incompressible flows using SPH," *J. Comput. Phys.*, vol. 136, no. 1, pp. 214–226, 1997.

[7] J. Brackbill, D. Kothe, and C. Zemach, "A continuum method for modeling surface tension," *J. Comput. Phys.*, vol. 100, no. 2, pp. 335–354, 1992.

[8] C. Chang and E. Franses, "Adsorption dynamics of surfactants at the air/water interface: a critical review of mathematical models, data, and mechanisms," *Colloids Surf. A*, vol. 100, pp. 1–45, 1995.

[9] J. Zhang, D. Eckmann, and P. Ayyaswamy, "A front tracking method for a deformable intravascular bubble in a tube with soluble surfactant transport," *J. Comput. Phys.*, vol. 214, no. 1, pp. 366–396, 2006.

[10] S. Yon and C. Pozrikidis, "A finite-volume/boundary-element method for flow past interfaces in the presence of surfactants, with application to shear flow past a viscous drop," *Computers & Fluids*, vol. 27, no. 8, pp. 879–902, 1998.

[11] J. Lee and C. Pozrikidis, "Effect of surfactants on the deformation of drops and bubbles in Navier-Stokes flow," *Computers & Fluids*, vol. 35, no. 1, pp. 43–60, Jan. 2006.

[12] G. Tryggvason, B. Bunner, A. Esmaeeli, D. Juric, N. Al-Rawahi, W. Tauber, J. Han, S. Nas, and Y. J. Jan, "A front-tracking method for the computations of multiphase flow," *J. Comput. Phys.*, vol. 169, no. 2, pp. 708–759, May 2001.

[13] X. Hu and N. Adams, "An incompressible multi-phase SPH method," *J. Comput. Phys.*, vol. 227, no. 1, pp. 264–278, 2007.

[14] S. Adami, X. Hu, and N. Adams, "A new surface tension formulation for multi-phase SPH using a reproducing divergence approximation," *J. Comput. Phys.*, vol. In Press, Accepted Manuscript, 2010.

[15] X. Hu and N. Adams, "A multi-phase SPH method for macroscopic and mesoscopic flows," *J. Comput. Phys.*, vol. 213, no. 2, pp. 844–861, 2006.

[16] I. Sbalzarini, J. Walther, M. Bergdorf, S. Hieber, E. Kotsalis, and P. Koumoutsakos, "PPM - a highly efficient parallel particle-mesh library for the simulation of continuum systems," *J. Comput. Phys.*, vol. 215, no. 2, pp. 566–588, 2006.

[17] G. Taylor, "The formation of emulsions in definable fields of flow," *Proc. Roy. Soc. London Ser. A*, pp. 501–523, 1934.

[18] J. Biddiscombe, D. Graham, and P. Maruzewski, "Visualization and analysis of SPH data," *ERCOFTAC Bulletin*, vol. 76, pp. 9–12, 2008.